Abiotic Formation of Alkylsulfonic Acids in Interstellar Analog Ices and Implications for their Detection on Ryugu

Mason McAnally[1,2], Jana Bocková[3], Ashanie Herath[1,2], Andrew M. Turner[1,2], Cornelia Meinert[3]*, Ralf I. Kaiser[1,2]*

[1]Department of Chemistry, University of Hawaii at Mānoa, Honolulu, HI 96822

[2]W.M. Keck Laboratory in Astrochemistry, University of Hawaii at Mānoa, Honolulu, HI 96822

[3]Université Côte d'Azur, Institut de Chimie de Nice, UMR 7272 CNRS, 06108 Nice, France

*Corresponding authors:

Cornelia.MEINERT@univ-cotedazur.fr, ralfk@hawaii.edu.

Supplementary Note 1

Two additional absorptions were assigned to carbon disulfide (CS_2), i.e., the asymmetric stretch (v_3) at 1520 cm^{-1} and the $v_1 + v_3$ combination mode at 2166 cm^{-1} [1]. The presence of carbonyl sulfide (OCS) is supported by the fundamental v_1 at 2042 cm^{-1} [1]. Finally, ethane (C_2H_6) was assigned via the v_5 fundamental at 2882 cm^{-1}, the v_{10} mode at 2977 cm^{-1}, the v_{11} at 1465 cm^{-1}, and the $v_8 + v_{11}$ combination band at 2941 cm^{-1} [2-4].

Isotopic shifting allowed for confirmation of small molecules, e.g., v_3 of CS_2 was observed at 1521 cm^{-1} in the non-labeled experiment, while a new peak at 1460 cm^{-1} appears in the SO_2/$^{13}CH_4$ ice consistent with $^{13}CS_2$ [1]. Consequently, since CS_2 contains no hydrogen, no shifting is detected in the SO_2/CD_4 experiment for CS_2.

Supplementary Note 2

Changes in the infrared spectra during irradiation were kinetically fit to provide insight into formation mechanisms initiated by energetic electrons[5]. The column densities (molecules cm^{-2}) of the reactants and products were determined utilizing a modified Beer-Lambert equation[6] and the corresponding integrated absorption coefficients (Supplemntary Table 12) during the irradiation (Fig. 5). The changes in column density of each reactant and product are summarized in Supplemntary Table 13 and the kinetic scheme utilized in these fits are cataloged in Supplemntary Table 14 as well as rate constants for each reaction in each dose.

A set of coupled differential equations were solved numerically under the assumption that the reactions followed elementary first and second-order growth and decay profiles. By combining first-order decay and second-order decay reactions, the column density of SO_2 was fit during irradiation.

The column density of sulfur dioxide (v_3, 1330 cm^{-1}) declines during irradiation, with the high dose experiment showing an 85% reduction in column density (-1.6×10^{17} molecules cm^{-2})— over five times larger than the low dose experiment (-2.9×10^{16} molecules cm^{-2}). The 1000 nA and 5000 nA experiments also included the reformation of SO_2 via radical-radical recombination of SO and atomic oxygen. The rate constant of the decomposition of SO_2 to SO and atomic oxygen is markedly higher in the 5000 nA experiment (5.3×10^{-5} s^{-1}) compared to the 100 nA experiment

(5.7×10^{-6} s^{-1}). The reduction in column density of methane—tracked by v_2 at 1300 cm^{-1}—during the irradiation occurs in all three dose experiments, and the most substantial change appears in the high dose experiment where the column density changes from 1.9×10^{17} molecules cm^{-2} to 4.3×10^{16} molecules cm^{-2}. Utilizing a similar scheme to SO$_2$, the decay of methane was fit along with an additional second-order decay to form unknown products in the 5000 nA experiment. This decrease in column density of methane coincides with an increase in the column density of the methyl radical (v_3, 3160 cm^{-1}) in the low dose experiment and the production of ethane (v_{10}, 2976 cm^{-1}) in the low, medium, and high dose experiments. The methyl radical is consumed predominately by radical-radical recombination to form ethane. The 5000 nA experiment shows the highest rate of ethane production of 2.8×10^{-17} cm^2 molecules^{-1} s^{-1}.

Since the 100 nA experiment provides identification of the methyl radical, the kinetic scheme was first fit utilizing these data. The formation of known intermediates such as SO$_3$ and the methyl radical reveals a possible pathway towards forming alkylsulfonic acids (ASAs). Sulfur trioxide— contains two second-order growths: the addition of atomic oxygen to SO$_2$ and a biomolecular reaction of SO$_2$ producing SO and SO$_3$. Two decay reactions are derived from the kinetic scheme. The first is a first-order decay towards unknown products. In the second, SO$_3$ reacts with the methyl radical to form CH$_3$SO$_3$. This reaction shows an order of magnitude increase between the 100 nA and 1000 nA experiments and between the 1000 nA and 5000 nA experiments. Previous computational work has described this reaction (Supplemntary Figure 8), where CH$_3$SO$_3$ initially goes through a van der Waals complex before a 1 kJ mol^{-1} barrier transition state[7]. Matrix effects and suprathermal reactants may allow the crossing of this minor barrier. After forming CH$_3$SO$_3$, hydrogen addition produces methylsulfonic acid. Since the band strengths of ASAs are unknown, the fits were completed by estimating the S=O stretching strength which was 5.0×10^{-17} cm molecule^{-1} before normalizing the fit to experimental data. This kinetic scheme accurately predicts the delay in the production of methylsulfonic acid (MSA) in the 100 nA experiment and the more rapid productions observed in the 1000 nA and 5000 nA experiments. Additionally, the rates derived for hydrogen addition to CH$_3$SO$_3$ show an increase from 1.2×10^{-19} cm^2 molecules^{-1} s^{-1} in the 100 nA experiment to 9.0×10^{-18} cm^2 molecules^{-1} s^{-1}, i.e., a 75 times increase in reaction rate.

This kinetic scheme represents one of the first attempts at understanding the production of organosulfur compounds in interstellar analog ices. This scheme provides insight into possible formation mechanisms of ASAs in SO_2/CH_4 ices and produces reaction rates applicable to interstellar icy mantles. Here, the synthesis of methylsulfonic acid occurs through methyl radical addition to sulfur trioxide before hydrogen addition to form MSA.
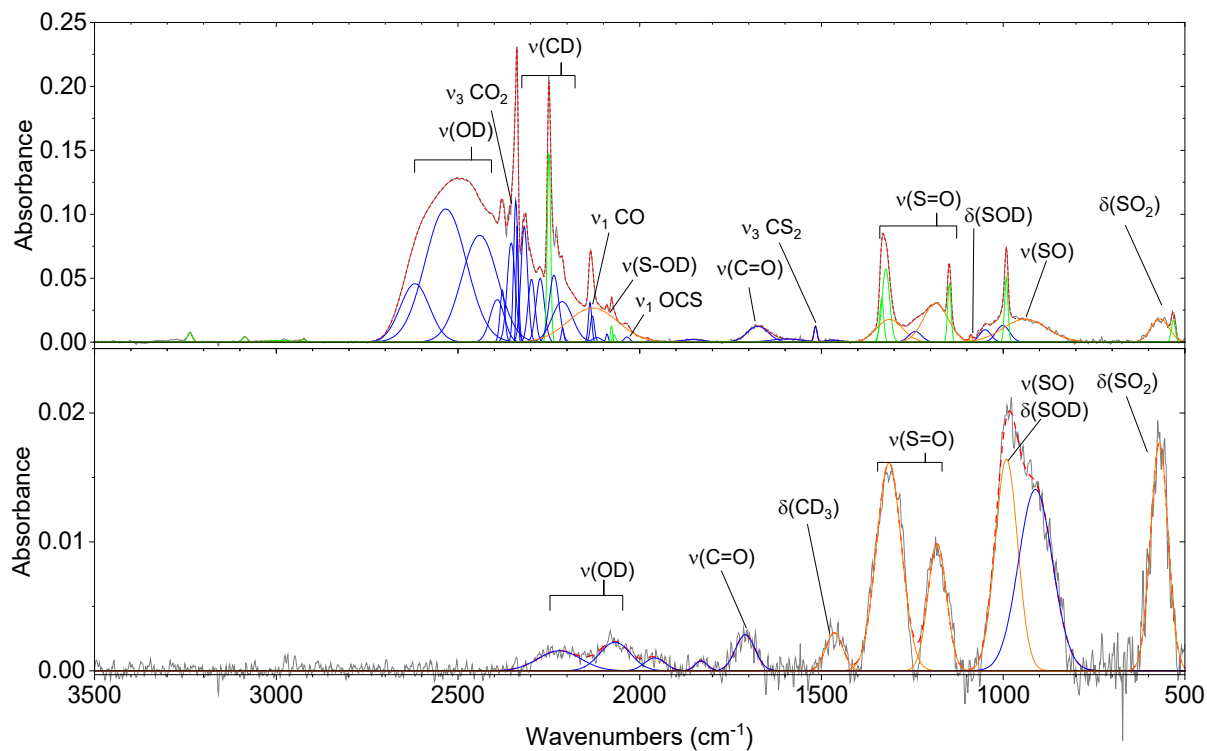
Supplementary Note 3

Changes in the infrared spectra collected during TPD (Supplemntary Figure 7) can reveal the sublimation temperature of compounds as well as thermal reactions. The TPD profiles indicate a decrease in column density starting at 30 K for methane and ethane, while SO_2 and SO_3 decrease at 110 K. The peak at 1200 cm^{-1} assigned to S=O stretching associated with compounds such as ASAs shows a decrease in signal at 250 K during the TPD in the low and medium dose experiments. The high dose experiment shows two increases in intensity starting at 150 K and 210 K and two decreases in signal at 170 K and 300 K. The changes in intensity in the high dose experiment suggest thermal reactions may play a notable role in the chemistry of these sulfur-containing ices and could contribute to the formation of ASAs.
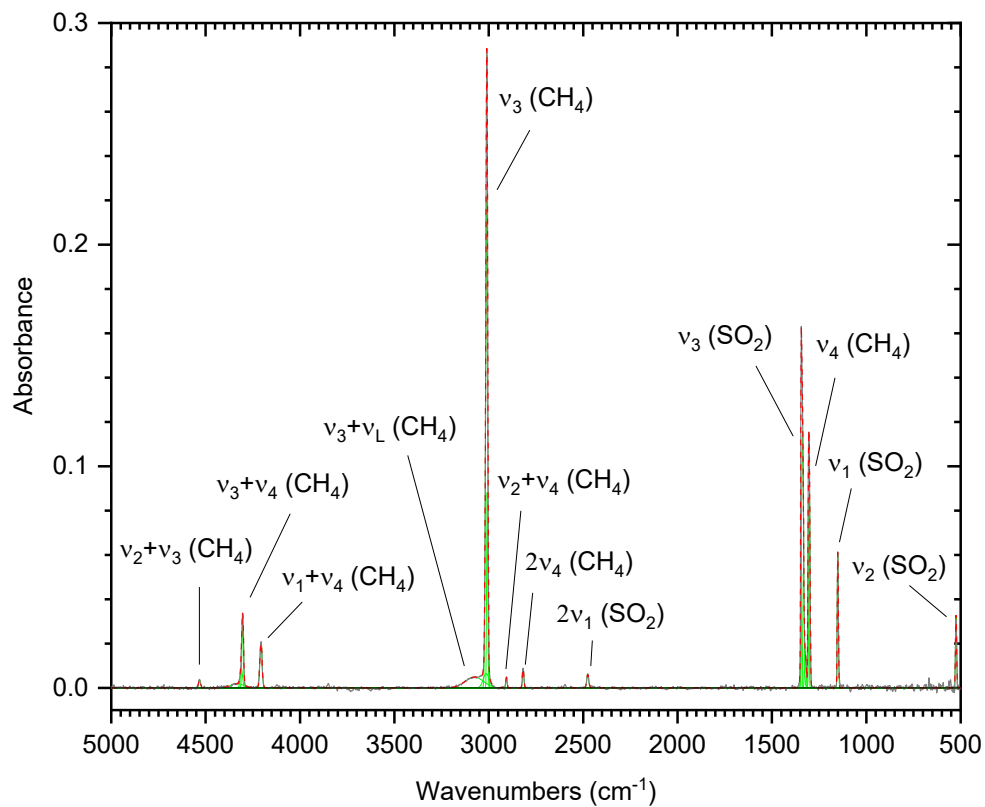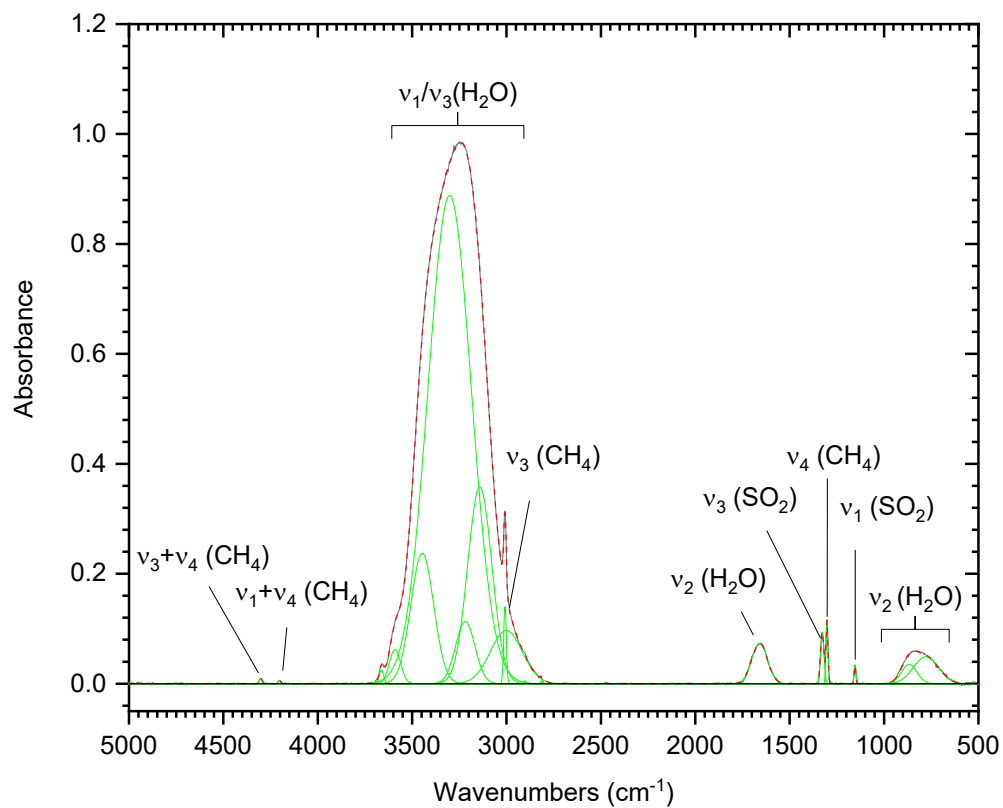
Supplementary Figure 1. Infrared spectra of SO_2/CH_4 ice at 10 K before irradiation. The original spectrum (gray) is deconvoluted showing peaks associated with reagents (green). These deconvolution peaks sum to the peak fitted spectrum (red dashed).
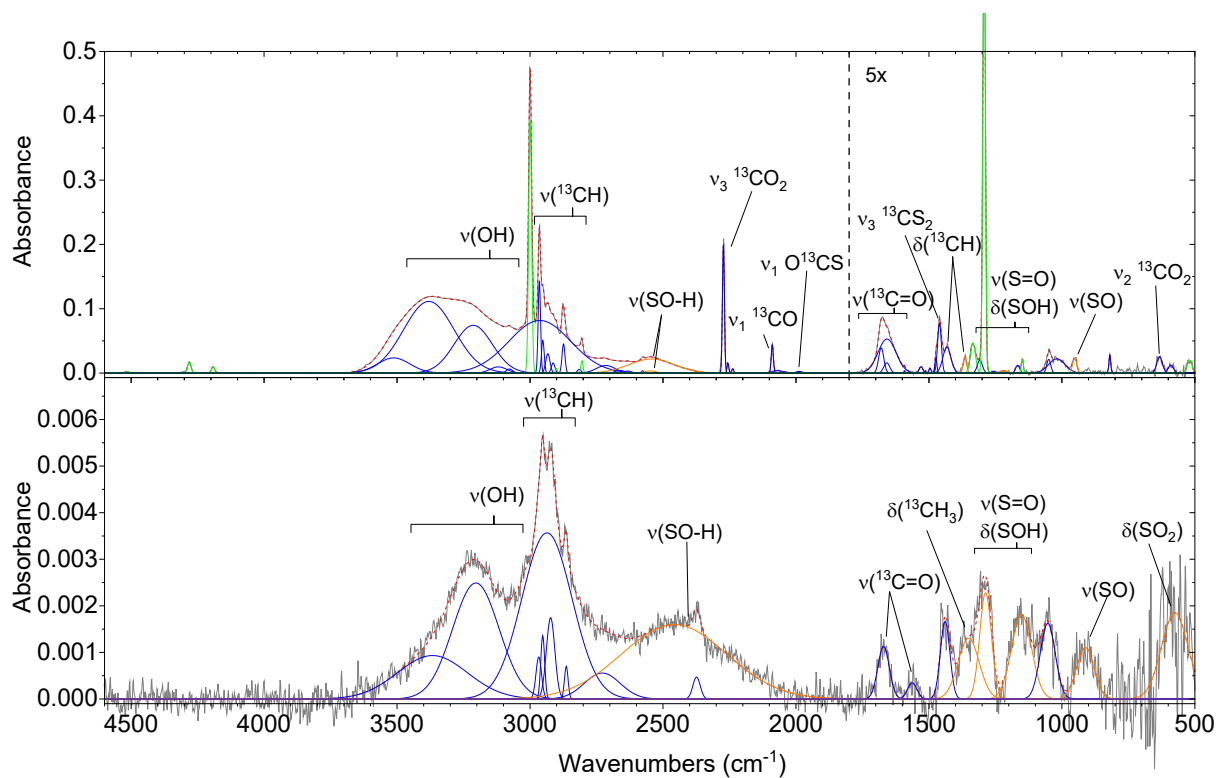
Supplementary Figure 2. Infrared spectra of $SO_2/^{13}CH_4$ ice at 10 K after irradiation (top) and at 320 K (bottom). The original spectrum (gray) is deconvoluted showing peaks associated with reagents (green), peaks associated with alkylsulfonic acids (orange) and other irradiation products (blue). These deconvolution peaks sum to the peak fitted spectrum (red dashed). Peak positions and assignments for after irradiation can be found in Supplementary Table 7 and for the residue in Supplementary Table 8.

Supplementary Figure 3. Infrared spectra of SO_2/CD_4 ice at 10 K after irradiation (top) and at 320 K (bottom). The original spectrum (gray) is deconvoluted showing peaks associated with reagents (green), peaks associated with alkylsulfonic acids (orange) and other irradiation products (blue). These deconvolution peaks sum to the peak fitted spectrum (red dashed). Peak positions and assignments for after irradiation can be found in Supplementary Table 9 and for the residue in Supplementary Table 10.
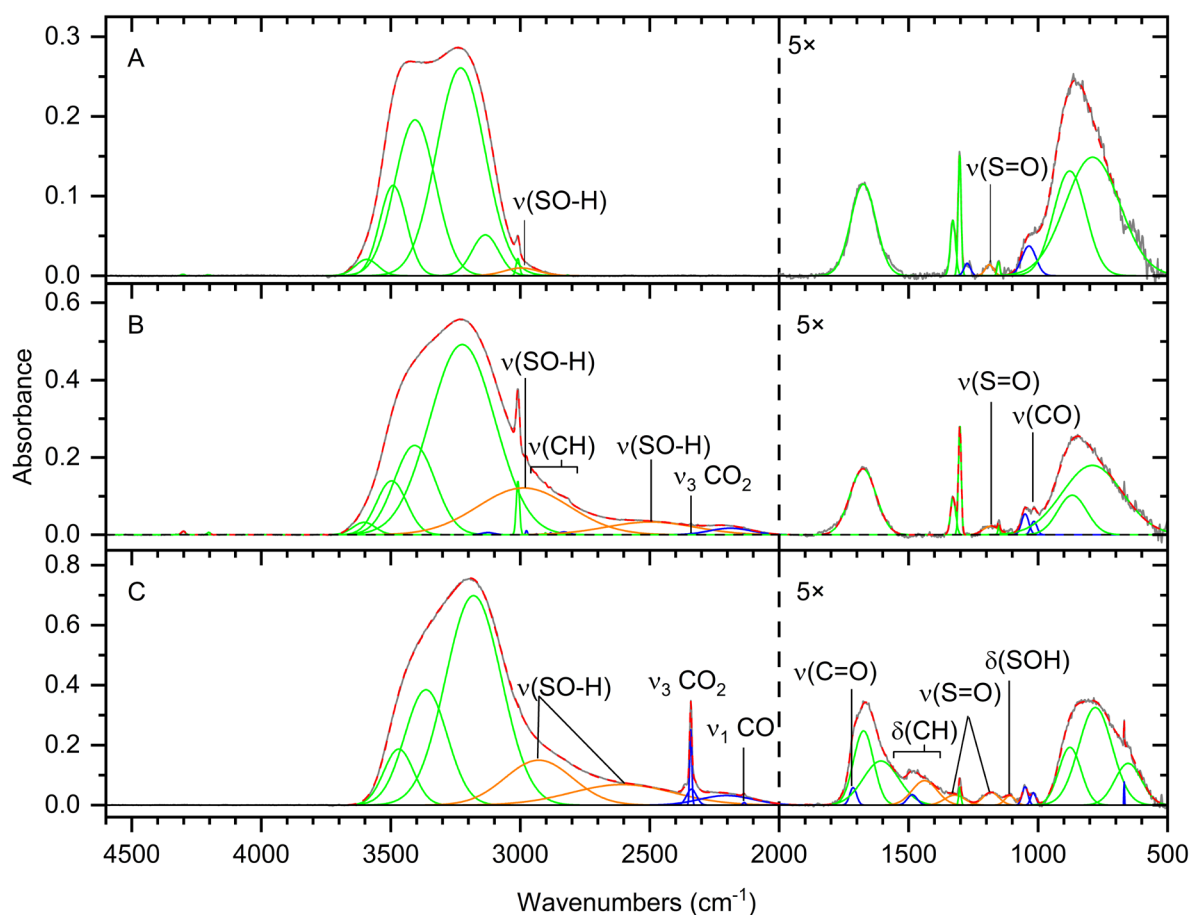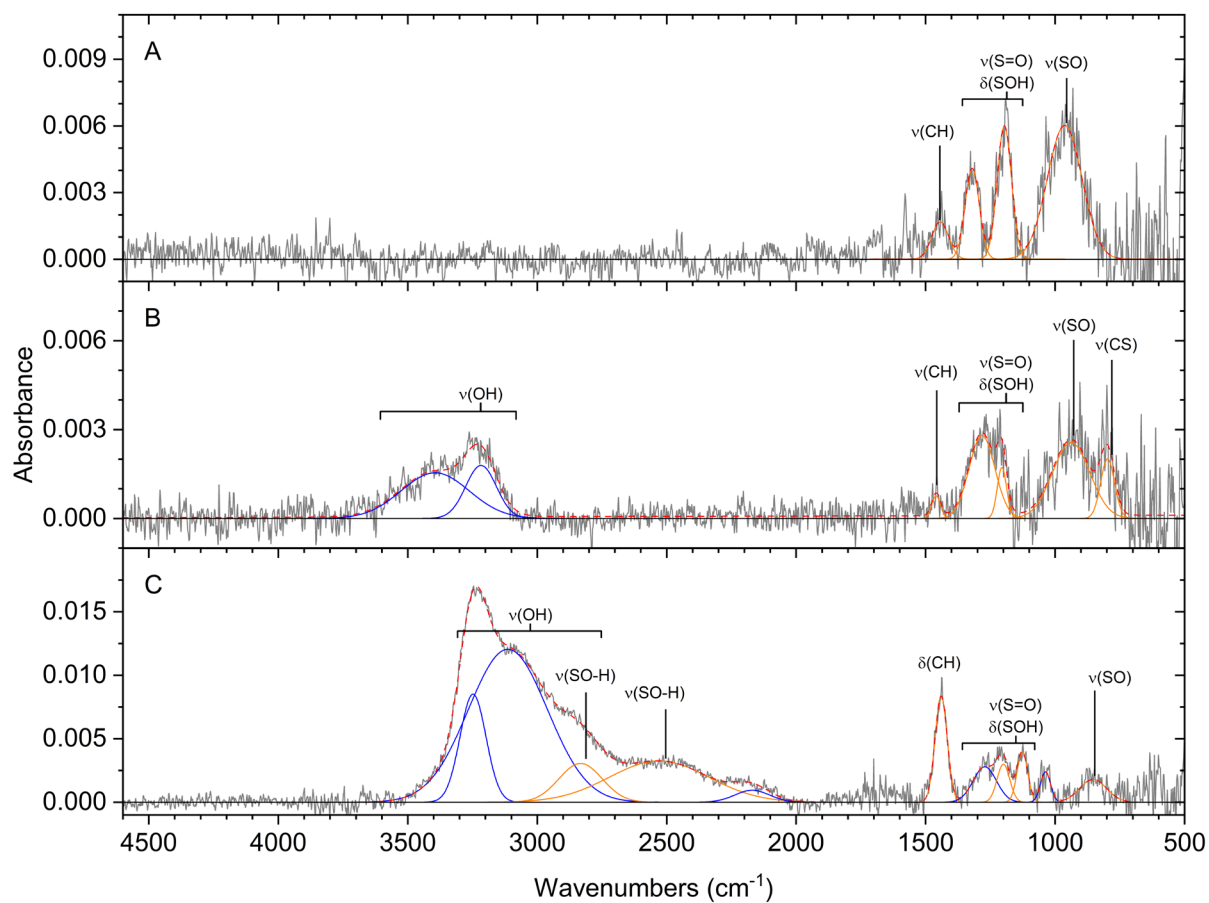
Supplementary Figure 4. Infrared spectra of $SO_2/H_2O/CH_4$ ice at 10 K before irradiation. The original spectrum (gray) is deconvoluted showing peaks associated with reagents (green). These deconvolution peaks sum to the peak fitted spectrum (red dashed).

Supplementary Figure 5. FTIR spectra of $SO_2/H_2O/CH_4$ ices at 10 K after irradiation for 1 hour at (A) 100 nA, (B) 1000 nA, and (C) 5000 nA current. The original spectrum (gray) is deconvoluted showing peaks associated with reagents (green), functional groups associated with alkylsulfonic acids (orange), and new irradiation products (blue). These deconvolutions sum to the peak fitted spectrum (red dashed). The data to the right of the dashed vertical line at 2000 cm^{-1} is magnified for clarity.
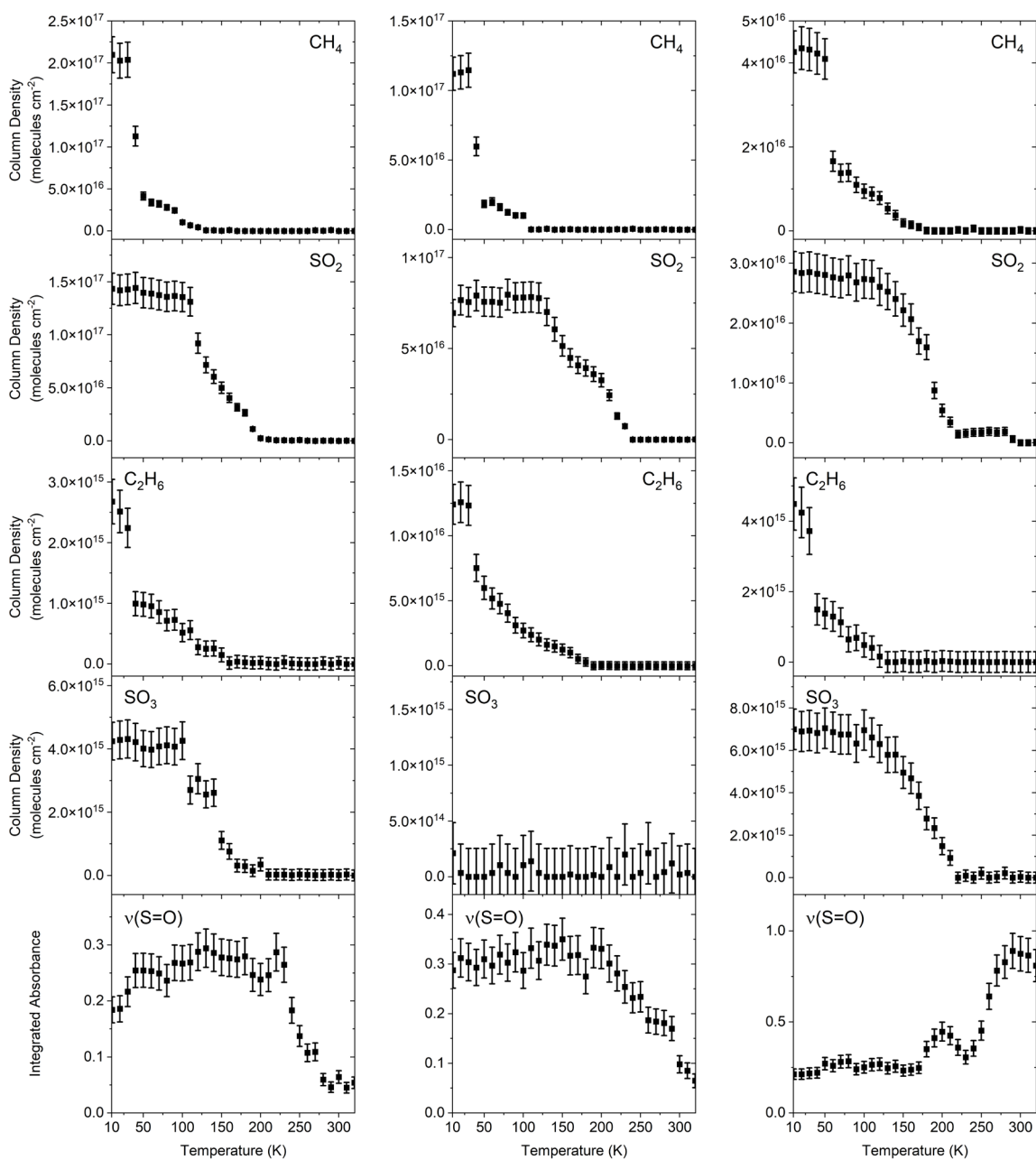
Supplementary Figure 6. FTIR spectra of $SO_2/H_2O/CH_4$ ices at 320 K after irradiation for 1 hour at (A) 100 nA, (B) 1000 nA, and (C) 5000 nA current. The original spectrum (gray) is deconvoluted showing functional groups associated with alkylsulfonic acids (orange), and new irradiation products (blue). These deconvolutions sum to the peak fitted spectrum (red dashed).

Supplementary Figure 7. Temporal evolution of selected infrared peaks during TPD in the SO₂/CH₄ experiments. The TPD profiles of selected infrared peaks of the low (left), medium (center), and high (right) dose. Methane, sulfur dioxide, ethane, sulfur trioxide, and v(S=O) were tracked by the 1300 cm^{-1}, 1330 cm^{-1}, 2976 cm^{-1}, 1380 cm^{-1}, and 1200 cm^{-1} peaks, respectively. Error bars are calculated from instrumental noise and error in ice thickness measurements.

Supplementary Table 1. Infrared absorption assignments for SO_2/CH_4 ices before irradiation.

Peaks before irradiation (10 K)		
Position (cm^{-1})	Identity	References
4533	$v_2 + v_3$ CH_4	2
4332	$v_3 + v_4$ CH_4	2
4311, 4303	$v_3 + v_4$ CH_4	2
4207	$v_1 + v_4$ CH_4	2
3077	$v_{3 + v_L}$ CH_4	2
3014, 3012, 3008	v_3 CH_4	2
2906	v_1 CH_4	2
2818	$v_2 + v_4$ CH_4	2
2476	$2v_1$ SO_2	8
1346, 1343, 1338, 1322	v_3 SO_2	8
1306, 1301	v_4 CH_4	2
1151	v_1 SO_2	8
524	v_2 SO_2	8

Note. "L" is used to define the lattice vibration

Supplementary Table 2. Infrared absorption assignments for SO_2/CH_4 experiments.

Position (cm^{-1})	Assignment	Dose (nA)	References	Position (cm^{-1})	Assignment	Dose (nA)	References
			Peaks after ir	radiation (10 K)			
4533	v_2+v_3 (CH$_4$)	100	2	2115	v(OH)	1000	9
4306	v_3+v_4 (CH$_4$)	100, 1000, 5000	2	2087	v(C≡C)	5000	9
4206	$v_1 + v_4$ (CH$_4$)	100, 1000, 5000	2	2037, 2042	v_1 (OCS)	1000, 5000	1
3849	v(OH)	100	9	1711, 1719	v(C=O)	100, 1000, 5000	9
3730, 3701	$v_1 + v_3$ (CO$_2$)	100, 1000, 5000	10	1695, 1689	v(C=O)	1000, 5000	9
3514–3629	v(OH)	100, 1000, 5000	9	1668	v(C=O)	5000	9
3399–3456	v(OH)	100, 1000, 5000	9	1619	v(C=O)	100	9
3207–3251	v(OH)	100, 1000, 5000	9	1521	v_3 (CS$_2$)	5000	1
3100, 3092	v(OH)	1000, 5000	9	1496	v(C=C), δ(CH)	1000, 5000	9
3049, 3069	v(OH)	100, 5000	9	1464, 1469	δ(CH), v_{11} C$_2$H$_6$	1000, 5000	2,9
3025	v(CH)	1000	9	1434	δ(CH)	5000	9
3008, 3010, 3018	v_3 CH$_4$	100, 1000, 5000	2	1396, 1382	v_3 (SO$_3$)	100, 5000	1
2978	v_{10} (C$_2$H$_6$)	100, 1000, 5000	2	1330	v_3 (SO$_2$)	100, 1000, 5000	8
2971	v(OH)	1000	9	1303	v_4 (CH$_4$)	100, 1000, 5000	2
2941	$v_8 + v_{11}$ (C$_2$H$_6$)	100, 1000, 5000	2	1270	v(S=O)	5000	9
2931, 2934	v(CH)	100, 5000	9	1241	v(S=O) SA	1000	11
2905	v_1 CH$_4$	100	2	1210	v(S=O) ASA, SA	1000, 5000	9,11-13
2899	v(SO-H) ASA	5000	9,12,13	1166, 1177	v(S=O)	100, 5000	9
2882	v_5 (C$_2$H$_6$)	100, 1000, 5000	2	1149	v_1 SO$_2$	100, 1000, 5000	8
2825	v(CH)	5000	9	1119	δ(SOH) ASA, SA	5000	9,11-13
2818	$v_2 + v_4$ (CH$_4$)	100, 1000, 5000	2	1100, 1103	v(S=O)	5000	9
2743, 2699	v(OH)	1000, 5000	9	1046, 1050	v(SO)	1000, 5000	9
2523–2588	v(SO-H) ASA	1000, 5000	9,12,13	961, 996	ρ(CH) ASA, v(SO) SA	1000	9,11-13
2476	v(C≡C)	100	9	887, 876	v(SO), ρ(CH)	1000	9,11
2409, 2447, 2437	v(OH)	1000, 5000	9	724, 786	v(CS) ASA	1000, 5000	9,12,13
2367	v(C≡C)	1000, 5000	9	679	OH Torsion	5000	9
2335, 2347, 2342	v_3 (CO$_2$)	100, 1000, 5000	10	668	v_2 (CO$_2$)	100, 1000, 5000	10
2276	v(C≡C)	1000	9	653, 656	δ(OH) alcohols	1000, 5000	9
2259, 2261	v(OH) acid	1000, 5000	9,11	577, 590	δ(SO)	1000, 5000	9
2234, 2237	v(C≡C)	100, 5000	9	526	v_2 (SO$_2$)	100, 1000	8
2166	$v_1 + v_3$ (CS$_2$)	5000	1				
2138	v_1 (CO)	100, 1000, 5000	1				

Note δ and ρ are used to describe the bending and rocking vibrational modes, respectively.

Supplementary Table 3. Infrared absorption assignments for SO_2/CH_4 experiments.

Infrared absorption assignments for SO_2/CH_4 experiments

	Residue (320 K)		
Position (cm^{-1})	Assignment	Dose (nA)	References
3410	v(OH)	100	9
3213, 3233, 3246	v(OH)	100, 1000, 5000	9
3073, 3056	v(OH)	1000, 5000	9
2845	v(SO-H) ASA	5000	9,11
2426	v(SO-H) ASA	1000	9
2377	v(C≡C)	5000	9
2323	v(C≡C)	1000, 5000	9
1725, 1730	v(C=O)	100, 5000	9
1700, 1695	v(C=O)	1000, 5000	9
1618, 1613	v(C=O)	100, 5000	9
1520, 1510, 1511	CH$_2$ scissoring, v(C=C)	100, 1000, 5000	9
1416, 1440	δ(CH) ASA	1000, 5000	9,12,13
1297	v(S=O) ASA	1000, 5000	9,12,13
1268	δ(OH) SA, v(S=O) ASA	100, 5000	9
1186	v(S=O) ASA, SA	1000	9,11-13
1116	δ(SOH) ASA, SA	5000	9,11-13
1045	v(CO)	1000, 5000	9
1023	v(CO)	5000	9
909, 864	ρ(CH) ASA, v(SO) SA	100, 5000	9,11-13
771	v(CS) ASA	1000, 5000	9,12,13
647, 621	δ(OH) alcohols	100, 5000	9

Supplementary Table 4. Infrared absorption assignments for $SO_2/^{13}CH_4$.

Position (cm^{-1})	Assignment	References	Position (cm^{-1})	Assignment	References
		Peaks after irradiation (10 K)			
4515	$v_2 + v_3\ ^{13}CH_4$	2	1679	$v(^{13}C{=}O)$	9
4281	$v_3 + v_4\ ^{13}CH_4$	2	1659	$v(^{13}C{=}O)$	9
4192	$v_1 + v_4\ ^{13}CH_4$	2	1658	$v(^{13}C{=}O)$	9
3513	$v(OH)$	9	1592	$v(^{13}C{=}O)$	9
3380	$v(OH)$	9	1530	$v(^{13}C{=}O)$	9
3214	$v(OH)$	9	1513	$v(^{13}C{=}O)$	9
3119	$v(OH)$	9	1496	$v(^{13}C{=}^{13}C), \delta(^{13}CH)$	9
3078	$v(OH)$	9	1474	$\delta(^{13}CH)$	9
3000	$v_3\ ^{13}CH_4$	2	1460	$v_3\ (^{13}CS_2)$	1
2965	$v_{10}\ ^{13}C_2H_6$	2	1433	$\delta(^{13}CH)$	9
2963	$v(OH)$	9	1365	$\delta(^{13}CH_3)$ ASA	9,12,13
2952	$v(^{13}CH)$	9	1335	$v_3\ SO_2$	8
2933	$v_8 + v_{11}\ ^{13}C_2H_6$	2	1309	$v(S{=}O)$	9
2913	$v(^{13}CH)$	9	1292	$v_4\ ^{13}CH_4$	2
2901	$v_1\ ^{13}CH_4$	2	1255	$v(S{=}O)$ SA, $\delta(SOH)$	11
2874	$v_5\ ^{13}C_2H_6$	2	1217	$v(S{=}O)$ ASA, SA	9,11-13
2815	$v(^{13}CH)$	9	1166	$v(S{=}O)$	9
2805	$v_2 + v_4\ ^{13}CH_4$	2	1149	$v_1\ SO_2$	8
2716	$v(OH)$	9	1050	$v(SO)$	9
2659	$v(^{13}CH)$	9	1019	$v(^{13}CO)$	9
2631	$v(^{13}CH)$	9	952	$\rho(CH_3)$ ASA, $v(SO)$	9,11-13
2576	$2v_4\ ^{13}CH_4$	2	820	$v(SO), \rho(CH)$	9
2547	$v(SO{-}H)$ ASA	9,12,13	633	$v_2\ ^{13}CO_2$	10
2544	$v(SO{-}H)$ ASA	9,12,13	591	$\delta(SO)$ ASA	9,12,13
2273	$v_3\ ^{13}CO_2$	10	520	$v_2\ SO_2$	8
2256	$v_3\ ^{13}CO_2$	10			
2238	$v(^{13}C{\equiv}^{13}C)$	9			
2089	$v_1\ (^{13}CO)$	10			
2070	$v(^{13}C{\equiv}^{13}C)$	9			
1988	$v_1\ (O^{13}CS)$	1			

Supplementary Table 5. Infrared absorption assignments for $SO_2/^{13}CH_4$.

	Residue (320 K)	
Position (cm^{-1})	Assignment	References
3367	$v(OH)$	9
3204	$v(OH)$	9
2967	$v(^{13}CH)$	9
2952	$v(^{13}CH)$	9
2936	$v(OH)$	9
2923	$v(^{13}CH)$	9
2864	$v(^{13}CH)$	9
2728	$v(OH)$	9
2458	$v(SO\text{-}H)$ ASA	9,12,13
2374	$v(^{13}C\equiv^{13}C)$	9
1671	$v(^{13}C=O)$	9
1563	$v(^{13}C=O)$	9
1439	$\delta(^{13}CH_3)$ ASA	9,12,13
1351	$\delta(^{13}CH_3)$ ASA	9,12,13
1287	$v(S=O)$ ASA, SA	9,11-13
1152	$\delta(SOH)$ ASA, SA	9,11-13
1053	$v(SO)$	9
912	$v(S\text{–}OH)$ ASA, SA	9,11-13
576	$\delta(SO_2)$ ASA	9,12,13

Supplementary Table 6. Infrared absorption assignments for SO_2/CD_4.

	Peaks after irradiation (10 K)				
Position (cm^{-1})	Assignment	References	Position (cm^{-1})	Assignment	References
3238	$v_3 + v_4$ CD$_4$	14	1468	δ(CD)	9
3087	$v_1 + v_4$ CD$_4$	14	1334	v_3 SO$_2$	8
2992	v_1 CHD$_3$	15	1323	v_3 SO$_2$	8
2926	$3v_4$ CD$_4$	14	1312	v(S=O) ASA	9,12,13
2618	v(OD)	9	1242	v(S=O) SA	11
2534	v(OD)	9	1185	v(S=O) ASA	9,12,13
2440	v(CD)	9	1148	v_1 SO$_2$	8
2392	v(OD)	9	1089	δ(SOD) ASA, SA	9,11-13
2378	v(CD)	9	1049	v(SO)	9
2354	v(CD)	9	1001	v(CO)	9
2341	v(CD)	9	991	v_4 CD$_4$	14
2337	v_3 CO$_2$	10	940	ρ(CH) ASA, v(SO) SA	9,11-13
2318	v(CD)	9	568	δ(SO$_2$) ASA	9,12,13
2298	v(CD)	9	532	v_2 SO$_2$	8
2274	v(CD)	9			
2250	v_3 CD$_4$	14			
2236	v_{10} C$_2$D$_6$	16			
2213	v(S-OD)	9			
2212	v(CD)	9			
2137	v_1 (CO)	10			
2130	v(C≡C)	9			
2129	v(OD)	9			
2118	v(C≡C)	9			
2090	v(C≡C)	9			
2078	v_5 C$_2$D$_6$	16			
2070	$v_2 + v_4$ CD$_4$	14			
2035	v_1 (OCS)	1			
1977	v(C≡C)	9			
1854	$v_3 + v_6$ C$_2$D$_6$	16			
1675	v(C=O)	9			
1596	v(C=O)	9			
1516	v_3 (CS$_2$)	1			

Supplementary Table 7. Infrared absorption assignments for SO_2/CD_4.

Position (cm^{-1})	Assignment	References
	Residue (320 K)	
2221	ν(OD)	9
2068	ν(OD)	9
1958	ν(C≡C)	9
1831	ν(C≡C)	9
1710	ν(C=O)	9
1465	δ(CD$_3$) ASA	9,12,13
1314	ν(S=O) ASA	9,12,13
1182	ν(S=O) ASA, SA	9,11-13
991	ν(S–OD) ASA, SA	9,11-13
911	ν(CO)	9
570	δ(SO$_2$) ASA	9,12,13

Supplementary Table 8. Infrared absorption assignments for $SO_2/H_2O/CH_4$ ices before irradiation.

Peaks before irradiation (10 K)		
Position (cm^{-1})	Identity	References
4302	v_3+v_4 CH$_4$	2
4203	v_1+v_4 CH$_4$	2
3662	OH Dangling H$_2$O	17
3591	v_1(O) H$_2$O	17
3446	v_3(L) H$_2$O	17
3301	v_3(L) H$_2$O	17
3218	v_3(T) H$_2$O	17
3142	v_1(T) H$_2$O	17
3008	v_3 CH$_4$	2
3001	v_1(I) H$_2$O	17
2902	v_1 CH$_4$	2
2818	v_2+v_4 CH$_4$	2
1659	v_2 H$_2$O	17
1327	v_3 SO$_2$	8
1302	v_4 CH$_4$	2
1154	v_1 SO$_2$	8
600-960	v_L H$_2$O	17
527	v_2 SO$_2$	8

Supplementary Table 9. Infrared absorption assignments for $SO_2/H_2O/CH_4$ experiments.

Position (cm⁻¹)	Assignment	Dose (nA)	References	Position (cm⁻¹)	Assignment	Dose (nA)	References
			Peaks After Irradiation (10 K)				
4302	$v_3 + v_4$ CH₄	100, 1000	2	1185	v(S=O) ASA, SA	100, 1000, 5000	9,11-13
4203	$v_1 + v_4$ CH₄	100, 1000	2	1152	v_1 SO₂	100, 1000	8
3593, 3603	OH Dangling	100, 1000	17	1109	δ(SOH) ASA	5000	9,12,13
3491, 3497,	v_l(O) H₂O	100, 1000, 5000	17	1051	v(SO)	1000, 5000	9
3406, 3408,	v_3(L) H₂O	100, 1000, 5000	17	1036	v(CO)	100	9
3299	v_3(L) H₂O	5000	17	1016, 1019	v(CO)	1000, 5000	9
3230, 3224	v_3(T) H₂O	100, 1000	17	868, 878, 877	v_L H₂O	100, 1000, 5000	17
3135, 3125,	v_l(T) H₂O	100, 1000, 5000	17	790, 790, 779	v_L H₂O	100, 1000, 5000	17
3125	v(OH)	1000	9	668	v_2 (CO₂)	5000	10
3008	v_3 CH₄	100, 1000, 5000	2	652	v_L H₂O	5000	17
2996	v(SO-H) ASA	100, 5000	9,12,13				
2987	v(OH)	1000	9				
2976	v_{10} C₂H₆	1000	2				
2938	$v_8 + v_{11}$ C₂H₆	1000	2				
2903	v(CH)	100, 1000	9				
2882	v_5 C₂H₆	1000	2				
2831	v(CH)	1000	9				
2817	v(OH) acid	100	9,11				
2815	v(CH)	1000	9				
2497, 2565	v(SO-H) ASA	1000, 5000	9,12,13				
2342	v_3 (CO₂)	1000, 5000	10				
2203	v(OH) acid	5000	9,11				
2189	$v_2 + v_4$ (CH₄)	1000	2				
2137	v_1 CO	1000, 5000	10				
1715	v(CO)	5000	9				
1676	v_2 H₂O	100, 1000, 5000	17				
1606	v(C=O)	5000	9				
1486	δ(CH)	5000	9				
1439	δ(CH) ASA	5000	9,12,13				
1329	v_3 SO₂	100, 1000, 5000	8				
1303	v_4 CH₄	100, 1000, 5000	2				
1274	δ(OH) SA	100	11				

Supplementary Table 10. Infrared absorption assignments for $SO_2/H_2O/CH_4$ experiments.

Position (cm^{-1})	Assignment	Dose (nA)	References
	Residue (320 K)		
3394, 3248	v(OH)	1000, 5000	9
3217, 3111	v(OH)	1000, 5000	9
2832	v(SO-H) ASA	5000	9,12,13
2528	v(SO-H) ASA	5000	9,12,13
2166	v(OH) acid	5000	9,11
1459, 1440	δ(CH) ASA	100, 1000, 5000	9,12,13
1320	v(S=O) ASA	100	9,12,13
1270, 1282	δ(OH) SA	100, 1000, 5000	9
1200	v(S=O) ASA, SA	100, 1000, 5000	9,11-13
1125	δ(SOH) ASA	5000	9,12,13
1036	v(CO)	5000	9
963, 938	ρ(CH) ASA, v(SO) SA	100, 1000	9,11-13
853	v(SO) ASA	5000	9,12,13
798	v(CS) ASA	1000	9,12,13

Supplementary Table 11. Identified alkylsulfonic acids as *tert*-butyldimethylsilyl derivatives by GC×GC–TOF-MS in the $SO_2/H_2O/CH_4$ and SO_2/CH_4 ice mixtures along with concentration estimates.

Compound	R_{t1} [a] (min)	R_{t2} [b] (sec)	$[M]^{+\bullet}$	$[M-57]^{+\bullet}$	$SO_2/H_2O/CH_4$ (nmol)			SO_2/CH_4 (nmol)		
					Low Dose	Medium Dose	High Dose	Low Dose	Medium Dose	High Dose
Methylsulfonic acid $CH_3SO_2(OH)$	17.17	1.48	210	153	10^{-1}	10^{-1}	10^{-1}	5×10^{-1}	5×10^{-1}	5×10^{1}
Ethylsulfonic acid $CH_3CH_2SO_2(OH)$	19.00	1.23	224	167	5×10^{-2}	5×10^{-2}	5×10^{-2}	5×10^{-2}	5×10^{-2}	5×10^{-1}
1-Propylsulfonic acid $CH_3CH_2SO_2(OH)$	20.92	1.19	238	181	n.d.	n.d.	10^{-3}	n.d.	10^{-3}	5×10^{-2}
Sulfuric Acid (H_2SO_4)	25.50	0.8	n.d.	269	n.d.	n.d.	10^{-1}	n.d.	10^{-1}	10^{1}

Note. n.d. is not detected
[a] GC×GC retention time 1st dimension.
[b] GC×GC retention time 2nd dimension.

Supplementary Table 12. Optical constants for small molecules tracked during irradiation and TPD in the infrared spectra.

Molecule	Position (cm^{-1})	A (cm molecule^{-1})	Reference
CH_4	1303	9.71×10^{-18}	18
SO_2	1333	1.47×10^{-17}	19
C_2H_6	2976	2.2×10^{-17}	20
CH_3	3160	2.88×10^{-18}	21
SO_3	1385	3.0×10^{-17}	22
MSA	1200	5.0×10^{-17}	estimated

MSA: methylsulfonic acid

**Supplementary Table 13.** Change in column density before and after irradiation of the SO_2/CH_4 ices.

| Identity | Change in column density (molecule cm^{-2}) | | |
	Low Dose	Medium Dose	High Dose
CH_4	-6.1×10^{16}	-7.4×10^{16}	-1.5×10^{17}
SO_2	-2.9×10^{16}	-1.3×10^{17}	-1.6×10^{17}
C_2H_6	2.6×10^{15}	1.3×10^{16}	4.3×10^{15}
SO_3	3.4×10^{15}	0.0	7.0×10^{15}
CH_3	0.0	n.d.	n.d.

Note n.d. is not detected.

Supplementary Table 14. Rate constants derived from iterative fitting of reaction scheme.

Reaction		Dose			Units
		100 nA	1000 nA	5000 nA	
SO_2	$\rightarrow SO + O(^3P/^1D)$	$5.7 \pm 1.3 \times 10^{-6}$	$6.8 \pm 1.0 \times 10^{-6}$	$5.3 \pm 1.1 \times 10^{-5}$	s^{-1}
$SO_2 + O(^3P/^1D)$	$\rightarrow SO_3$	$8.2 \pm 2.5 \times 10^{-22}$	$2.0 \pm 0.7 \times 10^{-22}$	$3.65 \pm 0.05 \times 10^{-22}$	$cm^2\ molecule^{-1}\ s^{-1}$
$[SO_2]_2$	$\rightarrow SO + SO_3$	$1.3 \pm 0.1 \times 10^{-22}$	$7.0 \pm 0.2 \times 10^{-22}$	$4.0 \pm 0.3 \times 10^{-22}$	$cm^2\ molecule^{-1}\ s^{-1}$
CH_4	$\rightarrow CH_3 + H(^2S)$	$1.0 \pm 0.5 \times 10^{-5}$	$2.3 \pm 0.3 \times 10^{-4}$	$9.5 \pm 0.3 \times 10^{-4}$	s^{-1}
$[CH_4]_2$	$\rightarrow CH_3 + CH_3 + 2H/H_2$	$1.27 \pm 0.05 \times 10^{-23}$	$8.6 \pm 2.1 \times 10^{-22}$	$8.25 \pm 0.07 \times 10^{-22}$	$cm^2\ molecule^{-1}\ s^{-1}$
$SO_3 + CH_3$	$\rightarrow CH_3SO_3$	$7.2 \pm 0.8 \times 10^{-20}$	$7.2 \pm 0.5 \times 10^{-19}$	$6.0 \pm 1.5 \times 10^{-18}$	$cm^2\ molecule^{-1}\ s^{-1}$
$CH_3SO_3 + H$	$\rightarrow CH_3SO_2(OH)$	$1.2 \pm 0.4 \times 10^{-19}$	$7.5 \pm 3.4 \times 10^{-19}$	$9.0 \pm 1.4 \times 10^{-18}$	$cm^2\ molecule^{-1}\ s^{-1}$
$CH_3 + CH_3$	$\rightarrow C_2H_6$	$8.1 \pm 0.2 \times 10^{-19}$	$5.6 \pm 0.8 \times 10^{-20}$	$2.8 \pm 0.3 \times 10^{-17}$	$cm^2\ molecule^{-1}\ s^{-1}$
$CH_3 + H(^2S)$	$\rightarrow CH_4$	-	$7.9 \pm 0.5 \times 10^{-20}$	$9.0 \pm 3.5 \times 10^{-18}$	$cm^2\ molecule^{-1}\ s^{-1}$
$SO + O(^3P/^1D)$	$\rightarrow SO_2$	-	$2.5 \pm 0.2 \times 10^{-20}$	$2.5 \pm 0.2 \times 10^{-20}$	$cm^2\ molecule^{-1}\ s^{-1}$
$CH_3SO_2(OH)$	$\rightarrow Products$	-	$4.3 \pm 0.6 \times 10^{-20}$	$3.0 \pm 0.2 \times 10^{-4}$	$cm^2\ molecule^{-1}\ s^{-1}$
CH_3	$\rightarrow Products$	$5.9 \pm 1.1 \times 10^{-3}$	$5.9 \pm 1.1 \times 10^{-3}$	$5.9 \pm 1.1 \times 10^{-3}$	s^{-1}
SO_3	$\rightarrow Products$	$8.7 \pm 0.3 \times 10^{-4}$	$9.5 \pm 2.0 \times 10^{-3}$	$3.0 \pm 1.0 \times 10^{-3}$	s^{-1}
$[SO_2]_2$	$\rightarrow Products$	-	-	$2.65 \pm 0.08 \times 10^{-21}$	$cm^2\ molecule^{-1}\ s^{-1}$
$[CH_4]_2$	$\rightarrow Products$	-	-	$1.7 \pm 0.4 \times 10^{-21}$	$cm^2\ molecule^{-1}\ s^{-1}$
$C_2H_6 + SO$	$\rightarrow Products$	-	-	$2.5 \pm 0.3 \times 10^{-18}$	$cm^2\ molecule^{-1}\ s^{-1}$
SO	$\rightarrow Products$	-	-	$2.0 \pm 1.0 \times 10^{-3}$	s^{-1}
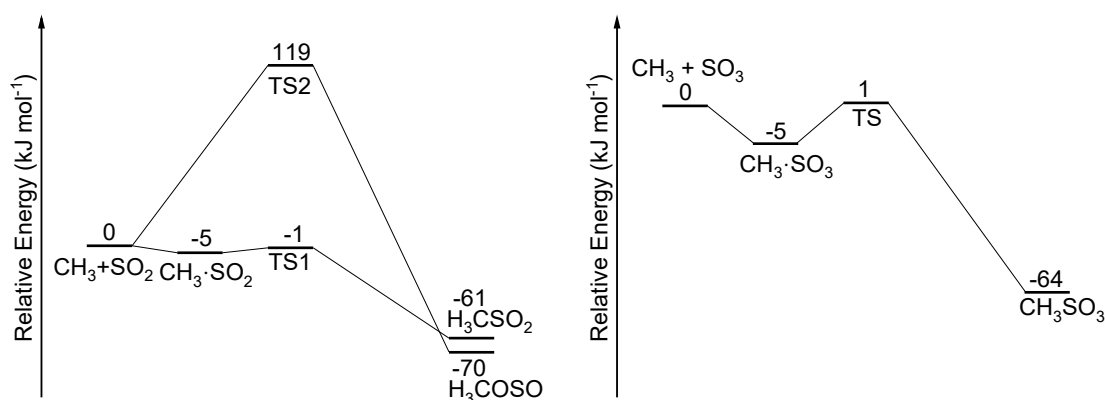
Supplementary Figure 8. Calculated potential energy surfaces for $SO_2 + CH_3$ and $SO_3 + CH_3$.
Radical addition of $CH_3^\bullet$ to SO_2 computed at the CCSD(T)/aug-cc-pV(Q+d)Z//CCSD(T)/6-311++G(2df, p) level (left) calculated by Ratliff et al.[23] and CH_3 addition to SO_3 computed at the G3XMP2//B3LYP/6-311+G(3df,2p) level of theory by Cao et al[7].

Supplementary References

1   Maity, S. & Kaiser, R. I. Electron irradiation of carbon disulfide–oxygen ices: Toward the formation of sulfur-bearing molecules in interstellar ices. *Astrophys. J.* **773**, 184, (2013).

2   Bennett, C. J., Jamieson, C. S., Osamura, Y. & Kaiser, R. I. Laboratory studies on the irradiation of methane in interstellar, cometary, and solar system ices. *Astrophys. J.* **653**, 792, (2006).

3   Gerakines, P. A., Schutte, W. A. & Ehrenfreund, P. Ultraviolet processing of interstellar ice analogs. I. Pure ices. *Astron. Astrophys.* **312**, 289–305, (1996).

4   Hepp, M. & Herman, M. Weak combination bands in the 3-μm region of ethane. *I. Mol. Spectrosc.* **197**, 56-63, (1999).

5   Turner, A. M., Abplanalp, M. J., Blair, T. J., Dayuha, R. & Kaiser, R. I. An Infrared Spectroscopic Study Toward the Formation of Alkylphosphonic Acids and Their Precursors in Extraterrestrial Environments. *Astrophys. J. Suppl.* **234**, 6, (2018).

6   Turner, A. M. *et al.* A photoionization mass spectroscopic study on the formation of phosphanes in low temperature phosphine ices. *Phys. Chem. Chem. Phys.* **17**, 27281–27291, (2015).

7   Cao Jia, W. W.-l., Gao Lou-jun, Fu feng. Mechanism and Thermodynamic Properties of CH_3SO_3 Decomposition. *Acta Physico-Chimica Sinica* **29**, 1161–1167, (2013).

8   Moore, M. H. Studies of proton-irradiated SO_2 at low temperatures: Implications for lo. *Icarus* **59**, 114–128, (1984).

9   Socrates, G. *Infrared and Raman Characteristic Group Frequencies*. 3rd edn, (2004).

10   Gerakines, P. A., Schutte, W. A., Greenberg, J. M. & van Dishoeck, E. F. The infrared band strengths of H_2O, CO and CO_2 in laboratory simulations of astrophysical ice mixtures. *Astron. Astrophys.* **296**, 810, (1995).

11   Zhong, L. & Parker, S. F. Structure and vibrational spectroscopy of methanesulfonic acid. *Royal Soc. Open Sci.* **5**, 181363, (2018).

12   Durig, J. R., Zhou, L., Schwartz, T. & Gounev, T. Fourier transform Raman spectrum, vibrational assignment and ab initio calculation of methanesulfonic acid in the gas and liquid phases. *J. Raman Spectrosc.* **31**, 193–202, (2000).

13   Nash, K. L., Sully, K. J. & Horn, A. B. Observations on the interpretation and analysis of sulfuric acid hydrate infrared spectra. *J. Phys. Chem. A* **105**, 9422–9426, (2001).

14   Calvani, P., Lupi, S. & Maselli, P. The infrared spectrum of solid CD_4. *J. Chem. Phys.* **91**, 6737–6742, (1989).

15   He, J., Gao, K., Vidali, G., Bennett, C. J. & Kaiser, R. I. Formation of molecular hydrogen from methane ice. *Astrophys. J.* **721**, 1656, (2010).

16   Abplanalp, M. J. & Kaiser, R. I. Complex hydrocarbon chemistry in interstellar and solar system ices revealed: A combined infrared spectroscopy and reflectron time-of-flight mass spectrometry analysis of ethane (C_2H_6) and d6-ethane (C_2D_6) ices exposed to ionizing radiation. *Astrophys. J.* **827**, 132, (2016).

17   Hagen, W., Tielens, A. & Greenberg, J. The infrared spectra of amorphous solid water and ice Ic between 10 and 140 K. *Chem. Phys.* **56**, 367–379, (1981).

18   Gerakines, P. A. & Hudson, R. L. Infrared spectra and optical constants of elusive amorphous methane. *Astrophys. J. Lett.* **805**, L20, (2015).

19   Garozzo, M., Fulvio, D., Gomis, O., Palumbo, M. E. & Strazzulla, G. H-implantation in SO_2 and CO_2 ices. *Planet. Space Sci.* **56**, 1300–1308, (2008).

20   Hudson, R. L., Gerakines, P. A. & Moore, M. H. Infrared spectra and optical constants of astronomical ices: II. Ethane and ethylene. *Icarus* **243**, 148–157, (2014).

21   Snelson, A. Infrared matrix isolation spectrum of the methyl radical produced by pyrolysis of methyl iodide and dimethyl mercury. *J. Phys. Chem.* **74**, 537–544, (1970).

22   Garozzo, M., Fulvio, D., Kanuchova, Z., Palumbo, M. E. & Strazzulla, G. The fate of S-bearing species after ion irradiation of interstellar icy grain mantles. *A&A* **509**, A67, (2010).

23   Ratliff, B. J., Tang, X., Butler, L. J., Szpunar, D. E. & Lau, K.-C. Determining the $CH_3SO_2 \rightarrow CH_3+SO_2$ barrier from methylsulfonyl chloride photodissociation at 193 nm using velocity map imaging. *J. Chem. Phys.* **131**, 044304, (2009).